

# Flexible Hybrid Electronics for Wireless Communication

*Carol Baumbauer*



Electrical Engineering and Computer Sciences  
University of California at Berkeley

Technical Report No. UCB/EECS-2019-162

<http://www2.eecs.berkeley.edu/Pubs/TechRpts/2019/EECS-2019-162.html>

December 1, 2019

Copyright © 2019, by the author(s).  
All rights reserved.

Permission to make digital or hard copies of all or part of this work for personal or classroom use is granted without fee provided that copies are not made or distributed for profit or commercial advantage and that copies bear this notice and the full citation on the first page. To copy otherwise, to republish, to post on servers or to redistribute to lists, requires prior specific permission.

**Flexible Hybrid Electronics for Wireless Communication**

by

Carol Baumbauer

A thesis submitted in partial satisfaction of the

requirements for the degree of

Master of Science

in

Electrical Engineering and Computer Science

in the

Graduate Division

of the

University of California, Berkeley

Committee in charge:

Professor Ana C. Arias, Chair

Professor Jan Rabaey

Spring 2019

---

**Flexible Hybrid Electronics for Wireless Communication**

by Carol Baumbauer

---

**Research Project**

Submitted to the Department of Electrical Engineering and Computer Sciences,  
University of California at Berkeley, in partial satisfaction of the requirements for the  
degree of **Master of Science, Plan II**.

Approval for the Report and Comprehensive Examination:

**Committee:**



---

Professor Ana C. Arias  
Research Advisor

05/16/2019

---

(Date)

\*\*\*\*\*



---

Professor Jan Rabaey  
Second Reader

05/15/2019

---

(Date)

**Flexible Hybrid Electronics for Wireless Communication**

Copyright 2019  
by  
Carol Baumbauer

## Abstract

Flexible Hybrid Electronics for Wireless Communication

by

Carol Baumbauer

Master of Science in Electrical Engineering and Computer Science

University of California, Berkeley

Professor Ana C. Arias, Chair

Printed flexible electronics have many applications in sensor networks, including wearable health monitoring. Wireless communication is an important aspect of nodes of a sensor network. Passive RFID is one approach well suited for communication with flexible sensors. A flexible passive RFID tag includes a printed antenna and an RF integrated circuit (RFIC). This report describes both printed antennas and RFIC integration. First, antennas fabricated with four different printing techniques—inkjet printing, spray coating, stencil printing, and screen printing—are compared. It is found that inkjet printed antennas have high losses because of their thinness while the other three techniques have similar performance. Next, materials and techniques for mounting rigid components such as the RFIC are discussed. Finally, complete functional tags operating in the UHF RFID band are demonstrated by sending data from on-board temperature sensors. These tags have a read range of up to 40 cm.

# Contents

<b>Contents</b>	<b>i</b>
<b>List of Figures</b>	<b>ii</b>
<b>List of Tables</b>	<b>iv</b>
<b>1 Introduction</b>	<b>1</b>
<b>2 Printing Technology</b>	<b>2</b>
2.1 Ink . . . . .	2
2.2 Printing Techniques . . . . .	3
<b>3 Printed Folded Dipole Antennas</b>	<b>6</b>
3.1 Antenna Design . . . . .	6
3.2 Materials and Methods . . . . .	6
3.3 Thickness and roughness . . . . .	7
3.4 DC Conductivity . . . . .	10
3.5 AC Performance . . . . .	11
3.6 RF performance . . . . .	12
<b>4 Flexible Hybrid Electronic Systems</b>	<b>18</b>
4.1 Conductive Adhesive Materials . . . . .	18
4.2 Mounting Mechanisms . . . . .	20
4.3 Impedance Matching . . . . .	21
4.4 Mounting Process . . . . .	23
<b>5 Complete RFID Tags</b>	<b>24</b>
5.1 RSSI and read range . . . . .	24
5.2 Temperature Measurements . . . . .	26
<b>Bibliography</b>	<b>30</b>

# List of Figures

2.1	a) In inkjet printing, ink is deposited drop by drop from a cartridge. b) In spray coating ink is applied as an aerosol, and pattern features are defined with a stencil. c) In stencil printing ink is applied with a blade in direct physical contact with the pattern-defining stencil. d) In screen printing ink is forced through a patterned mesh screen with a squeegee. . . . .	3
3.1	a) Inkjet printed traces have a very smooth surface. Bumps in the edges of the lines come from spreading of individual drops of ink. b) Spray coated traces have rough edges from the peeled stencil and rough surface from the deposition as aerosol. c) Stencil printed traces have rough stencil edges and a smooth surface. d) Screen printed traces have clean edges, well defined features, and a moderately smooth surface. . . . .	8
3.2	a) Inkjet printed traces are less than $1 \mu m$ thick. b) Spray coated samples are about $5 \mu m$ thick and have significant surface roughness compared to total thickness. c) Stencil printed samples are about $40 \mu m$ thick and have large peaks at the edge of the traces. d) Screen printed samples are about $15 \mu m$ thick with considerable roughness. . . . .	9
3.3	Design and dimensions of folded dipole antenna pattern . . . . .	10
3.4	The $S_{11}$ Parameters of Screen Printed (dotted red lines) and Stencil Printed (solid blue lines) Antennas are nearly identical, and have strong resonance near 917 MHz. . . . .	13
3.5	$S_{11}$ Parameters of inkjet printed antennas show only weak resonance near 905 MHz. Printing two layers of ink improves the resonance. . . . .	14
3.6	$S_{11}$ Parameters different techniques printed antennas. Screen, stencil, and spray coated samples have similar performance and strong resonance. Inkjet printed samples clearly have weak resonance by comparison. . . . .	14
3.7	Gain different techniques Printed Antennas. All antennas have a peak gain at 915 MHz, and screen and stencil printed samples have nearly three times higher gain than inkjet printed samples . . . . .	16



4.1	a) Zero-ohm resistor mounted with low temperature solder. b) Zero-ohm resistor mounted with screen printable silver ink. c) Test traces connected to adapters for RF cables. . . . .	19
4.2	a) Contacts-up chip placement may need a ramp to prevent disconnected traces. b) Pick-and-place tools are used to align pads to traces for chips mounted contacts-down. . . . .	21
4.3	At low power, the IC impedance is about $1.5-58j \Omega$ , causing inefficient power transfer between a $50 \Omega$ reference and the IC. Mismatch efficiency of an IC on printed traces is similar to that of an IC on reference substrates. Insets: a) IC mounted on printed traces. b) The AMS rigid reference board. c) The flex PCB reference board; . . . . .	22
4.4	a) A laser cut stencil is used to define areas where the components will be attached to the traces. b) The wet ink after being stencil printed on the traces. c) The IC and matching network components mounted to the substrate. . . . .	23
5.1	Measurement set up for RSSI and read range. The interrogator antenna sends the radio signal to the passive tag and receives the response. Successful connections were established at distances up to 40 cm. . . . .	25
5.2	RSSI vs distance for printed and reference boards . . . . .	26
5.3	Two printed tags can send temperature data over the air to the interrogator antenna. All components of the wireless link are inside an environmental chamber. . . . .	27
5.4	a) The rigid reference board follows relative increases and decreases in temperature well, but temperature readings are influenced by relative humidity. The signal is noisier at high humidity. The Flex PCB signal is extremely noisy and contains errors of up to $100^\circ\text{C}$ . b) Both printed samples follow relative increases and decreases in temperature well and are only minorly impacted by humidity changes. Note that the printed samples were measured at two different times, which causes the small gap in the readings. Calibration would improve the absolute accuracy of the readings. . . . .	28

# List of Tables

2.1	Properties of silver inks for Inkjet, Spray, Stencil, and Screen printing . . . . .	3
3.1	DC resistance characteristics of inks and techniques . . . . .	11
3.2	Key parameters of RF performance of antennas made with different printing techniques. . . . .	15
4.1	Resistive losses at RF frequencies for several conductive adhesive materials . . .	20

## Acknowledgments

Many thanks to Dr. Arno Thielens for assistance and instruction on antenna characterization and performance in both practical and theoretical aspects. He also designed the antennas.

Thanks to Dr. Igal Deckman for preliminary work on antenna fabrication and chip mounting options, and for introducing me to printing techniques. Jonathan Ting assisted with screen printing and advising on printing techniques. Thanks also to members of the Arias research group for support and assistance.

This work has been supported by the Israel Ministry of Defense [IMOD]

This material is based, in part, on research sponsored by Air Force Research Laboratory under agreement number FA8650-15-2-5401, as conducted through the flexible hybrid electronics manufacturing innovation institute, NextFlex. The U.S. Government is authorized to reproduce and distribute reprints for Governmental purposes notwithstanding any copyright notation thereon. The views and conclusions contained herein are those of the authors and should not be interpreted as necessarily representing the official policies or endorsements, either expressed or implied, of Air Force Research Laboratory or the U.S. Government.

# Chapter 1

## Introduction

Flexible electronics enable large area, lightweight, thin functional devices. These flexible electronic devices are useful in Internet of Things applications as they enable interfacing electronics with complex physical objects. Flexible sensors are being developed in industries including automotive, packaging, and structural health monitoring. Wearable medical technology has seen considerable advancement in recent years in consumer health monitoring products like smart watches, and in research of clinical grade sensors. Sensors including temperature, heart rate, blood oxygenation, and various metabolites present in sweat have been demonstrated [1, 2, 3, 4, 5]. In all cases, to be truly “wearable” a device should be comfortable: conformal, lightweight, thin, and cable-less. A functional wearable device must include not only a sensor, but also a power source and communication ability [6, 7]. The power and communication systems should meet the same comfort criteria as the sensors.

Printed electronic components have the advantages of being flexible, lightweight, thin, and large area. Conventional rigid silicon electronics are capable of fast, efficient computation, data processing and storage in a small footprint at low power. Flexible hybrid electronic systems take advantage of these complementary strengths by integrating conventional components and printed components together [8].

Radio Frequency Identification (RFID) tags are an example of a commercially available flexible hybrid electronic system. Passive RFID tags are powered by the RF energy of an interrogator or reader antenna. The RFID tag is a simple device consisting of an antenna, which is typically a few centimeters in order to operate in the RF band, and a single chip with the tag’s ID number and sometimes information from sensors on the tag. Because of their simplicity and the large size of the antenna, printing is particularly well suited as a fabrication method for passive RFID tags [9].

# Chapter 2

## Printing Technology

### 2.1 Ink

There are many commercially available conductive inks that are specially formulated for each printing technique. In this work, all conductive inks were silver based, although gold, carbon, and polymer conductive inks are also available. Silver is commonly used in printed electronics for its higher conductivity than carbon and lower cost than gold. Silver inks are composed of silver nano particles or flakes and a polymer binder dissolved in a solvent. Sometimes small amounts of additives are used to improve specific properties, such as adhesion to specific substrates, or resistance to certain chemicals. Some important parameters of different types of ink are summarized in Table 2.1. Inkjet ink is a thin liquid with viscosity around 10-15 cps and solid content 30-40%. Surface tension of ink is an important characteristic for inkjet printing, and inks are developed to be compatible with specific printing processes. Spray coating ink is also a thin liquid with viscosity 50-100 cps and silver content 35-40%. Additives in spray coating ink can help with adhesion and mechanical flexibility. Screen printing ink (which can also be used for stencil printing) is a paste-like ink with high viscosity on the order of 30,000 cps and silver content  $> 80\%$  after curing. Varieties of screen printing ink are developed for adhesion to specific substrates, for very fine feature resolution, or for particularly high conductivity.

Because the silver in the inks is discrete, solid small particles, after printing the ink must be annealed. The heat dries the solvent and fuses the discrete silver particles together into a single conductive trace [10]. Samples can be annealed on a hotplate or in a vacuum oven. Annealing in a vacuum oven can help reduce oxidation of the metal. Optimal annealing temperatures range from 100-150°C, depending on the ink. The annealing temperature should not be above the glass transition temperature of the plastic substrate or the substrate will be deformed.

Printing Technique	Examples	Solid Content %	Typical Solvent	Viscosity cps	Resitivity $\mu\Omega$ cm	Sheet Resistivity $\Omega/\square/\text{mil}$
Inkjet	ANP DGP-40LT-15C Novacentrix JS-A102	30-40	TGME	8-17	6-12	0.2
Spray	Dupont 5069 Novacentrix PSPI-1000 Creative Materials 124-02	35-50	Water	50-100	8-100	0.5-.45
Stencil or Screen	Dupont 5064H Novacentrix HPS-FG57B Creative Materials 126-33, 118-09	> 70%		10,000-35,000	20-30	6-10

Table 2.1: Properties of silver inks for Inkjet, Spray, Stencil, and Screen printing

## 2.2 Printing Techniques

There are many types of solution processing fabrication techniques, each with their own strengths and weaknesses. In this work, inkjet printing, spray coating, stencil printing, and screen printing are used.

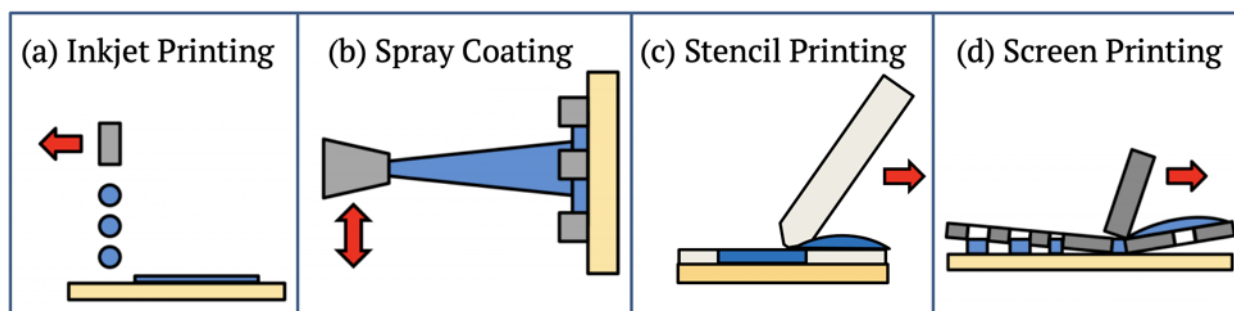


Figure 2.1: a) In inkjet printing, ink is deposited drop by drop from a cartridge. b) In spray coating ink is applied as an aerosol, and pattern features are defined with a stencil. c) In stencil printing ink is applied with a blade in direct physical contact with the pattern-defining stencil. d) In screen printing ink is forced through a patterned mesh screen with a squeegee.

## Inkjet Printing

In inkjet printing, ink is held in a cartridge which has a nozzle or nozzles that dispense the ink drop by drop onto the substrate as shown in Fig.2.1a. The nozzle uses a piezoelectric piece to control drop jetting [11]. Like an office printer, the pattern printed by an inkjet printer is digitally generated. This makes inkjet printing an attractive candidate for prototyping; the printing pattern is a digital file which can easily be modified. A disadvantage of inkjet printing is that, because patterns are produced drop by drop, it can be much slower than other printing options, especially when using research scale—rather than industrial scale—printers. Inkjet printing typically produces metal traces with thickness of a few hundred nanometers at most. Minimum feature size depends on drop volume, ink viscosity and chemistry, and substrate surface energy, but is generally in the range of 10 to 50  $\mu\text{m}$ . Surface chemistry can be modified with monolayer or plasma treatments to improve print quality and resolution for a specific ink [8].

## Spray Coating and Stencil Printing

Stencil printing and spray coating are two other prototyping techniques. In both cases, the pattern is defined by a stencil. In this work, stencils are made of six-inch wide Kapton (polyamide) tape. The tape is applied to the full substrate and the patterns are defined by a laser engraver which cuts the kapton stencil layer but not the underlying substrate. The areas of the pattern where ink will be are then removed with tweezers, which limits minimum feature size to about 1 mm. Because they are made of adhesive tape, masks are not reusable. However, designs can be easily changed from sample to sample by changing the CAD file used by the laser engraver, so these methods are well suited to prototyping.

Once the substrate with its mask is prepared, ink is applied through either spray coating or stencil printing. In spray coating, the ink is put in an air brush and comes out as an aerosol as shown in Fig.2.1b. Final layer thickness is determined by the distance between the brush and the substrate, the speed that the brush is moved across the substrate, the flow rate of air and ink, and the number of the passes of the brush over a certain area. Spraying can be controlled by an automatic sprayer, or done by hand.

In stencil printing, a viscous ink is used. It is spread across the top of the substrate and dragged with a blade (usually a glass slide or a razor blade) over the pattern as shown in Fig.2.1c. The thickness is set by the thickness of the stencil material since the blade is in contact with the stencil the whole time. Automated set ups can control the blade speed, or the blade can be moved by hand. Production by hand allows for fine tuning the angle between the blade and the substrate and the pressure of the blade in order to get a clean print, but can be less reproducible than automated printing.

## Screen Printing

The final printing technique used in this work is screen printing. Screen printing uses a mesh screen to define the pattern. These screens are specially made with emulsion layers and mesh size chosen based on the ink properties. A flood bar spreads the ink over the screen, then a squeegee forces the ink through the holes in the mesh, transferring the pattern onto the substrate as shown in Fig.2.1d [9]. This technique is very fast and scalable to roll to roll (R2R) processing. Minimum feature size is about 50  $\mu\text{m}$ . Thickness is determined by the ink and process parameters, such as ink viscosity, squeegee pressure, and screen height. and is generally on the order of 10's of  $\mu\text{m}$ . Screen printing is not suited to early prototype work because changing the design requires purchasing a new custom screen.



## Chapter 3

# Printed Folded Dipole Antennas

### 3.1 Antenna Design

The antennas are folded dipole antennas designed to radiate at 915 MHz, which is the center frequency of the UHF RFID band in the USA (902-928 MHz). Fig. 3.3 shows the pattern dimensions. The antenna is designed for free space operation and dimensions were chosen to be easily printed with any technique [12].

### 3.2 Materials and Methods

Several antennas with the same pattern were prepared using each of the techniques described above. All samples were printed on Q65HA, a 125  $\mu\text{m}$  thick polyethylene naphthalate (PEN) plastic film from Teijin Dupont. The screen printed and stencil printed samples were printed with 126-33 extremely conductive silver ink (Creative Materials, Ayer, MA, USA) and were annealed on a hot plate for 10 minutes at 130 °C unless otherwise noted. Adhesive Kapton stencils for spray and stencil coating were patterned using a 30 W Universal VLS2.30 desktop laser cutter (Universal Laser Systems Inc, Scottsdale, AZ, USA). The spray coated samples used PSPI-1000 ink (NovaCentrix, Austin, TX, USA) annealed in the vacuum oven at 130 °C for 15 minutes. Both stencil printing and spray coating were done by hand. The inkjet printed samples were printed with DGP 40LT-15C silver ink (Advanced Nano Products, Sejong, Korea). The prints were done with a 10 pL cartridge, drop spacing of 25  $\mu\text{m}$ , and platen temperature of 52°C. Samples were annealed in the vacuum oven at 140°C for one hour. Most inkjet samples were printed with a single layer; one was printed with two.

Several key parameters were compared between the four techniques, including edge roughness and minimum feature size, thickness and surface roughness, DC and AC resistive losses, and antenna gain.

### 3.3 Thickness and roughness

The printing technique influences edge roughness and surface texture as seen in Fig 3.1. The inkjet sample in Fig 3.1a has a smooth surface which appears dark under the microscope. There is a regular pattern to the edge roughness in the y-direction that is the result of ink spreading at the end of each printed line. The spray coated and stencil printed samples in Fig 3.1b and c have rough edges from the laser cut and peeled stencils. The spray coated sample's texture is quite rough. The screen printed sample in Fig 3.1d has the smoothest edges and most cleanly defined features.

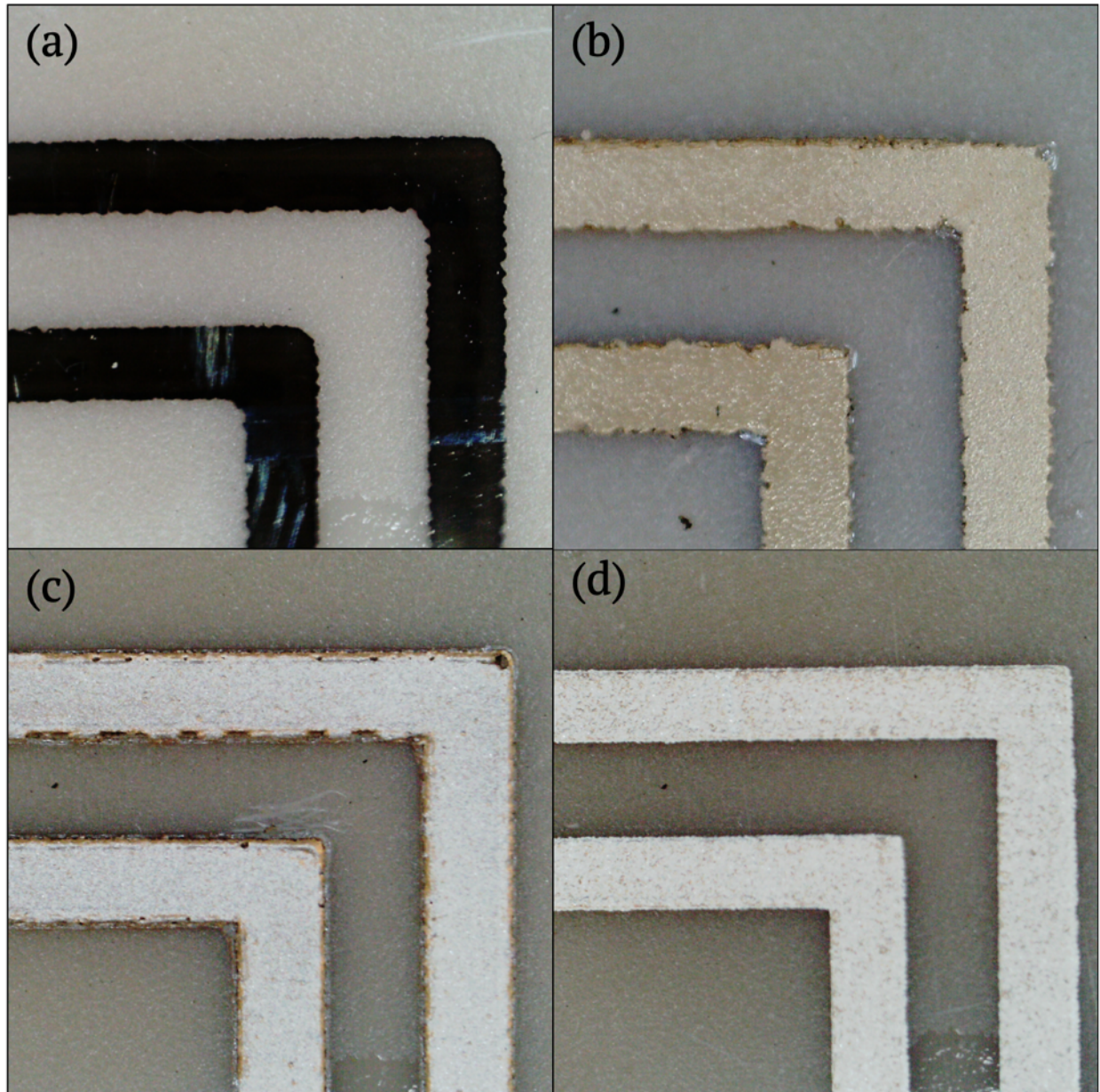


Figure 3.1: a) Inkjet printed traces have a very smooth surface. Bumps in the edges of the lines come from spreading of individual drops of ink. b) Spray coated traces have rough edges from the peeled stencil and rough surface from the deposition as aerosol. c) Stencil printed traces have rough stencil edges and a smooth surface. d) Screen printed traces have clean edges, well defined features, and a moderately smooth surface.

The surface roughness can also be seen in profiles of the printed traces for each technique.

The inkjet printed samples have a thin traces—on the order of a few hundred nanometers in most places, as seen in 3.2a. The average thickness is 250 nm, with most measurements

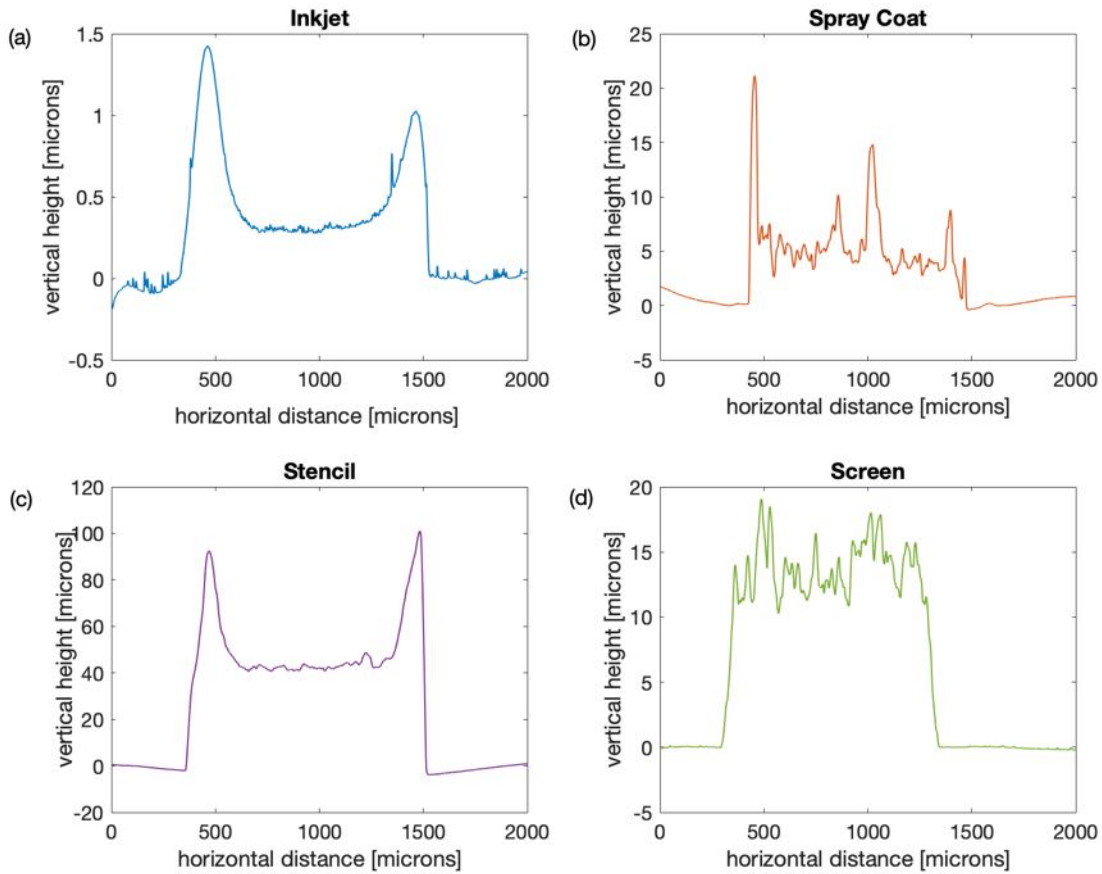


Figure 3.2: a) Inkjet printed traces are less than  $1 \mu m$  thick. b) Spray coated samples are about  $5 \mu m$  thick and have significant surface roughness compared to total thickness. c) Stencil printed samples are about  $40 \mu m$  thick and have large peaks at the edge of the traces. d) Screen printed samples are about  $15 \mu m$  thick with considerable roughness.

falling between 150-350 nm. The profile shown in 3.2a has an average thickness of 304 nm and standard deviation of 15.3 nm in the flat center portion. The edge peaks in the figure seem to be bubbles or places where ink is not well attached to the substrate.

The spray coated samples have average thickness of about  $4 \pm 2 \mu m$ . The example shown in 3.2b has an average thickness of  $5.4 \mu m$  and standard deviation of  $2.4 \mu m$ . Many samples have extremely large peaks on the edges, which is probably an artifact of the stencil edge. Most samples, including the one in 3.2b, have edge peaks of around 15-30  $\mu m$ , but a few samples have peaks as high as 90  $\mu m$  tall.

The stencil printed samples have a thickness of about  $40 \mu m$ , with 80-100  $\mu m$  peaks at the edges of the lines. Usually, these peaks appeared on both sides where ink dried while coating the stencil wall, as in the example shown in 3.2c. Some stencil print samples have a

peak only on one side, probably at the end of the pass. The example shown in 3.2 has an average thickness of  $43 \mu\text{m}$  and standard deviation of  $1.6 \mu\text{m}$  in the flat center part. Stencil printed samples have are the thickest with the lowest standard deviation relative to their thickness.

The screen printed samples have the least sample to sample variation and do not have edge peaks, as shown in Fig 3.2d. This sample has an average thickness of  $13.8 \mu\text{m}$  and standard deviation of  $2.0 \mu\text{m}$ .

### 3.4 DC Conductivity

The conductivity of the antennas was found by measuring the DC resistance between the two feeder points shown in Fig 3.3. In a good conductor, DC current flow is uniform across the entire cross sectional area of the conductor, and the resistance of a section of conductor is given by  $R = \rho \frac{L}{wt}$  where  $\rho$  is the bulk material resistivity in  $\Omega - m$ ,  $L$  the length,  $w$  the width and  $t$  the thickness. For thin conductors, the sheet resistance,  $R_s = \frac{\rho}{t}$ , in ohms per square [ $\Omega/\square$ ] is another common measure of conductivity that takes thickness into account.

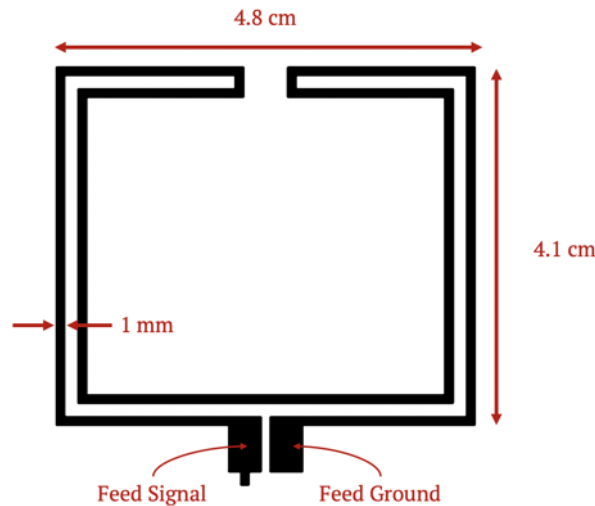


Figure 3.3: Design and dimensions of folded dipole antenna pattern

To see how these parameters can be calculated from DC resistance measurements and profile data, here is an example using a stencil printed sample. The DC resistance was measured from the contact points on the antenna and found to be  $5.7\Omega$ . The antenna trace width is 1 mm and the total path length between the contact points is 320 mm. Therefore the sheet resistance is  $5.7 \div 320 = 0.178\Omega/\square$ . The resistivity can be found by  $\rho = R_s t$  where  $R_s$  is the sheet resistance and  $t$  the thickness, about  $40\mu\text{m}$  for stencil printed devices. In this case, the resistivity is  $0.178 * 40\mu\text{m} = 7.12 \times 10^{-7}\Omega\text{m}$ . Conductivity data for the different printing techniques is given in Table 3.1.

Printing technique	Ink	Thickness	DC Resistance	Sheet Resistivity [ $\Omega/\square$ ]	Resistivity measured [ $\Omega - m$ ]	nominal ink resistivity [ $\Omega - m$ ]
Inkjet	ANP DGP-40LT-15C	250 nm	160 $\Omega$	0.5	1.25E-7	1.1-1.2E-7
Spray	Novacentrix PSPI-1000	4 $\mu m$	-	-	-	8.5E-7
Stencil print	Creative Materials 126-333	40 $\mu m$	5.7 $\Omega$	0.018	7.2E-7	2E-7
Screen print	Creative Materials 126-33	15 $\mu m$	9.1 $\Omega$	0.029	5.7E-7	2E-7

Table 3.1: DC resistance characteristics of inks and techniques

The annealing parameters have a significant influence on the final conductivity of any ink. For screen printed samples, annealing at 100 °C for 10 minutes yields resistance that is twice that of samples annealed for 10 minutes at 130 °C. Annealing at an even higher temperature could improve the conductivity to the  $2 \times 10^{-7} \Omega - m$  listed in product documentation.

From Table 3.1 it is clear that, although inkjet printing yields the highest conductivity, the extremely thin trances mean that overall resistance is more than a order of magnitude higher for inkjet printed samples than any of the other techniques.

### 3.5 AC Performance

Unlike DC current, AC current flow is concentrated at the edges of the conductor and exponentially decays further into the conductor. For a perfect conductor, all current flow is on the surface of the conductor [13]. In a good conductor, the current density,  $J(z)$  is given by (3.1)

$$J_x(z) = J_0 \exp(-\alpha z) \exp(-j\beta z) \quad (3.1)$$

Where  $J_0$  is the current density at the surface. The skin depth of a conductor is a way of measuring how far into the surface of a conductor an EM wave effectively propagates. It is defined as the depth where the electric field amplitude has dropped to  $1/e$  of its value at the surface. The skin depth of a good conductor is approximated by (3.2)

$$\delta_s = \frac{1}{\sqrt{(\pi f \mu \sigma)}} [m] \quad (3.2)$$

Ninety-nine percent of the current flow is contained within the first five skin depths; 95% of the current flow is contained within the first three skin depths. Therefore, for a printed

structure to effectively carry RF current, its thickness should be on the order of a few skin depths.

The skin depth can be calculated from the resistivity information in table 3.1. For the stencil printed sample in the example above, the skin depth is calculated using (3.2) with  $\sigma = \frac{1}{\rho}$ ,  $f = 915\text{MHz}$ , and  $\mu = \mu_0 = 4\pi \times 10^{-7}[\text{H}/\text{m}]$ . This gives  $\delta_s = 14 \mu\text{m}$ . Since the conductor thickness is  $40 \mu\text{m}$ , nearly three times the skin depth, we expect the thickness of the printed trace to not significantly limit the antenna performance.

For inkjet printing, the story is somewhat different. A typical inkjet printed sample has DC resistance of around  $160\Omega$  and thickness of about  $250 \text{ nm}$ , so the sheet resistance is  $0.5\Omega/\text{square}$  and resistivity is  $1.2 \times 10^{-7} \Omega - \text{m}$ . This gives a skin depth of about  $6 \mu\text{m}$  for a frequency of  $915 \text{ MHz}$ . However, inkjet printed traces are typically less than  $1 \mu\text{m}$  thick. The thinness of inkjet printed traces is likely to degrade their performance as antennas at these frequencies. Printing multiple layers makes thicker traces and reduces DC resistance. This was seen in the double-layer sample, whose DC resistance is about half that of the other inkjet printed samples. However, the resistivity and skin depth are material properties, and are not changed by thickness. In order to make an inkjet printed trace at least  $6 \mu\text{m}$  thick, it would need about 25 layers of ink, which is impractical in prototyping and small-batch scenarios.

### 3.6 RF performance

The antennas' RF performance is characterized by scattering parameters, or S-parameters, which were measured with a Vector Network Analyzer (VNA) (Agilent N5242A, PNA-X, Santa Clara, CA, USA). The VNA has two ports: it generates an RF signal with known voltage amplitude and phase at one port, then measures the received complex signal at both ports. The scattering parameters relate the applied signal to the returned signal. For example  $S_{11} = \frac{\widetilde{V}_1^-}{\widetilde{V}_1^+}$  where  $\widetilde{V}_1^+$  is the complex voltage wave applied at port one and  $\widetilde{V}_1^-$  is the complex voltage waveform received at port one. Naturally, the S-parameters are themselves complex numbers. The percent of power reflected back to the first port is  $|S_{11}|^2$ , and the percent of power transmitted to the second port is  $|S_{12}|^2$ . The VNA was set to sweep frequency from  $0.5$  to  $2.5 \text{ GHz}$  in steps of  $1 \text{ MHz}$ . A single antenna's RF performance is characterized by its S11 parameter. At frequencies where it is not radiating, S11 should be close to unity (or zero dB) indicating that most of the power is reflected, as it would be in an ideal short or open stub transmission line. At resonance, S11 should be very small (large negative values in dB), because most of the power is being radiated, not reflected. Some key performance metrics are the resonance frequency, which was designed to be  $915 \text{ MHz}$ , and the minimum S11 value, which should be as low as possible, and certainly below  $-10 \text{ dB}$ .

Both stencil and screen printed antennas performed well. All samples had resonance between  $910 \text{ MHz}$  and  $920 \text{ MHz}$ , and peak S11 loss of  $-16.9 \text{ dB}$  and  $-22.3 \text{ dB}$ . Out of resonance, S11 is between  $-3 \text{ dB}$  and  $0 \text{ dB}$ . The samples which were annealed at  $100 \text{ }^\circ\text{C}$  had higher



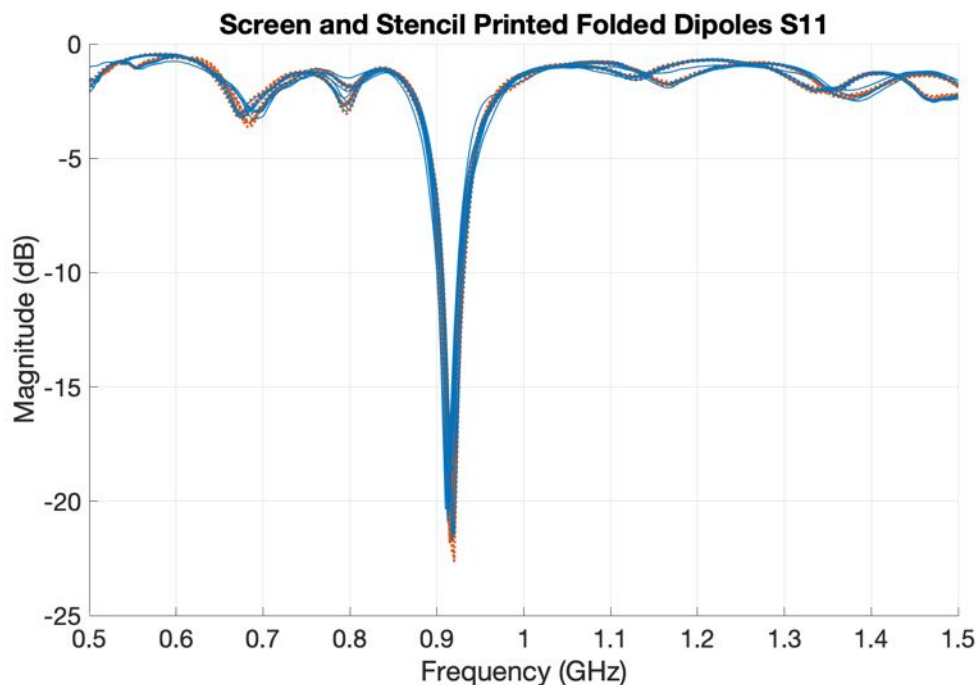


Figure 3.4: The S11 Parameters of Screen Printed (dotted red lines) and Stencil Printed (solid blue lines) Antennas are nearly identical, and have strong resonance near 917 MHz.

resistance and lower resonance peaks, about -17 dB, while those annealed at 130 °C had peaks of -20 to -22 dB. This was expected as the samples annealed at a higher temperature have lower DC resistance.

The performance of the screen and stencil printed antennas seen in Fig 3.4 is nearly identical. In these figures, all screen printed antennas are represented with dotted red lines, and all stencil printed antennas with solid blue lines. No significant difference between the printing techniques is visible.

By comparison, inkjet printed samples have much weaker and slightly shifted resonance peaks as seen in Fig 3.5. Average resonance frequency is 906 MHz, and the average minimum magnitude is -6.9 dB. The double layer sample had a peak of -9.8 dB at 910 MHz. None of these samples meet the goal of less than -10 dB in the resonance band. This is likely due to the extreme thinness of the inkjet printed traces.

The spray coated samples behave much like the screen and stencil printed antennas, but the spray coated samples have more variable performance. This is probably because the spray coated samples have more sample to sample variation in their thicknesses, and therefore their resistive losses.

When the average results from the four techniques are plotted together in Fig 3.6, it is clear that stencil, spray, and screen coating all agree well with simulation data, but inkjet printing does not.



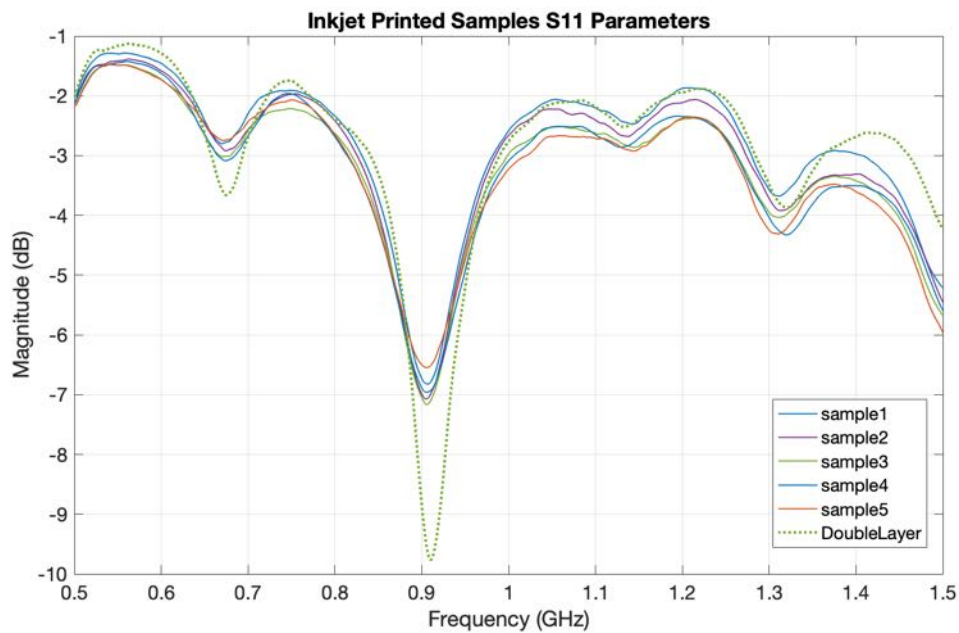


Figure 3.5: S11 Parameters of inkjet printed antennas show only weak resonance near 905 MHz. Printing two layers of ink improves the resonance.

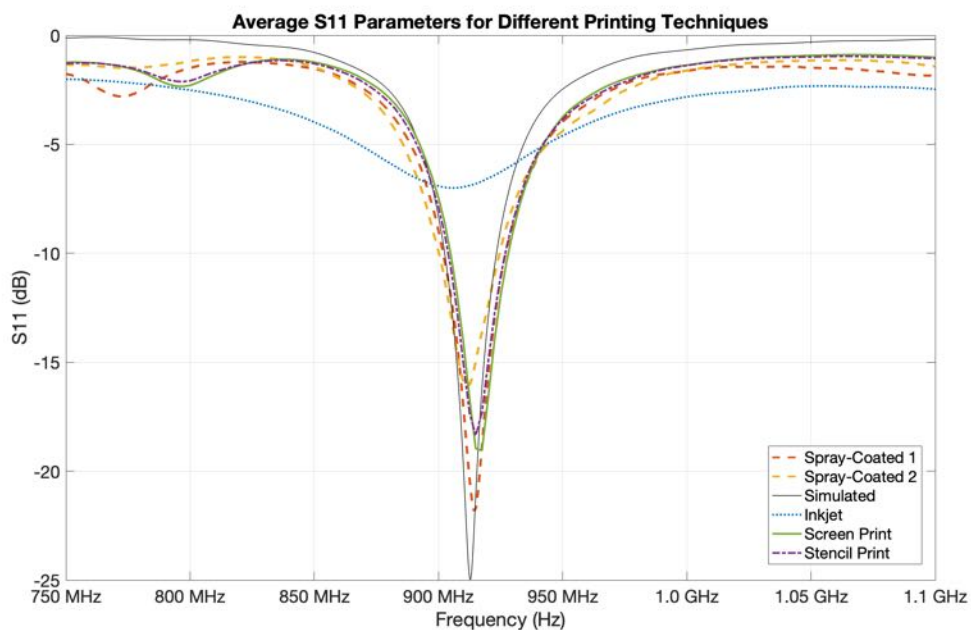


Figure 3.6: S11 Parameters different techniques printed antennas. Screen, stencil, and spray coated samples have similar performance and strong resonance. Inkjet printed samples clearly have weak resonance by comparison.

## Antenna Gain Measurements

The VNA can also be used to measure transmission between two antennas and thus their gain. To measure gain, the two antennas were mounted upright with their feed lines coming in from the bottom and their printed faces towards each other, with a fixed distance of 61 cm between them. In these measurements,  $|S_{12}|^2$  and  $|S_{21}|^2$  represent the fraction of power transmitted from one antenna to the other, and should be identical to each other. Losses from impedance mismatch, radiation efficiency, and propagation losses are all part of this power transfer term.

Power transmission in free space is governed by the Friis equation, 3.3.

$$\frac{P_R}{P_T} = G_1 G_2 \frac{\lambda^2}{(4\pi d)^2} \quad (3.3)$$

Where  $\frac{P_R}{P_T} = |S_{12}|^2$  is the fraction of received power,  $G_1$  and  $G_2$  are the gains of each antenna,  $\lambda$  is the wavelength, and  $d$  is distance between the antennas. In order to uniquely calculate the gain of a single antenna, three antennas must be measured in all three possible pairings. Each single instance of the Friis equation can be solved for the product  $G_1 G_2$ . With three instances using antennas 1, 2, and 3, the gains of the individual antennas can be found. Gain measurements were made for three inkjet printed antennas, three screen printed antennas, and three stencil printed antennas.

As expected from the S11 measurements, the inkjet antennas have much lower gain than the stencil printed and screen printed cases. Figure 3.7 shows antenna gains as a function of frequency for these three printing techniques. The screen printed case has slightly higher gain than stencil printed, but the variation within one technique is comparable to the difference between them, as shown in Table 3.2.

	Resonance Frequency	S11	Gain
Inkjet	906 ± .8 MHz	-6.9 ± .1dB	.215
Stencil	916 ± 3.4 MHz	-20.4 ± 1.2 dB	.745 ± .02
Screen	916 ± 2.4 MHz	-20.5 ± 2 dB	.807 ± .09

Table 3.2: Key parameters of RF performance of antennas made with different printing techniques.

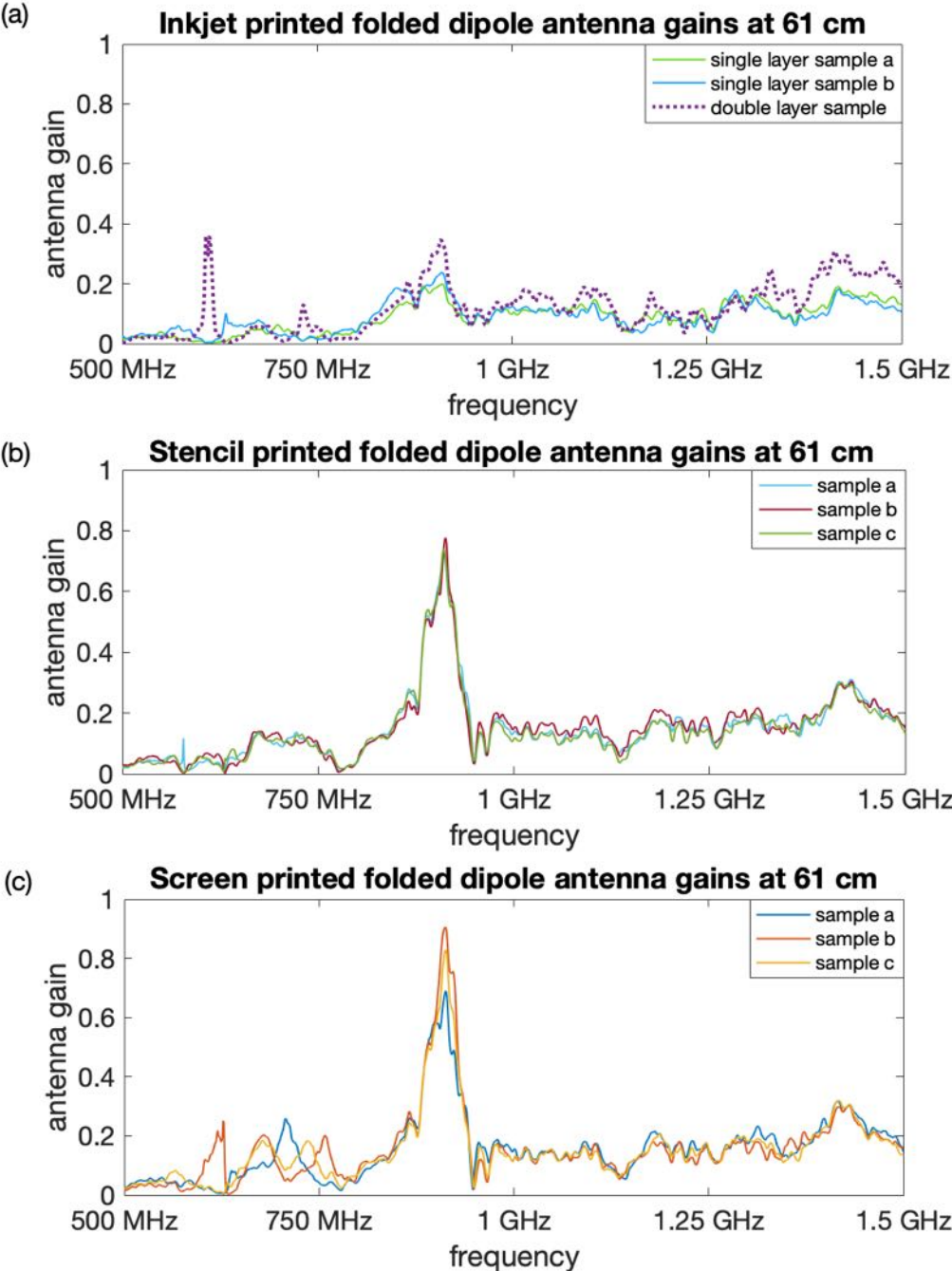


Figure 3.7: Gain different techniques Printed Antennas. All antennas have a peak gain at 915 MHz, and screen and stencil printed samples have nearly three times higher gain than inkjet printed samples

Although inkjet printed antennas have been demonstrated in the literature [11, 14, 15], the very thin nature of inkjet printed traces makes this a non-ideal fabrication technique for antennas. For prototyping or small-batch production, stencil and spray coating are both good choices. Stencil printing produces thicker and more repeatable results than spray coating when both are done by hand. For large batch production screen printing is the best option because of the ease of production and comparable performance to stencil printing. Another advantage of screen printing is its finer feature resolution, which is important for flexible hybrid electronic systems.

## Chapter 4

# Flexible Hybrid Electronic Systems

Antennas are an important part of wireless communication systems, but they are only one part. Addressing abilities and interconnects to sensors are also necessary capabilities of a functional RFID tag. These services are most effectively provided by conventional rigid components. In this work, a complete RFID tag consists of three or four parts: the printed antenna, an impedance matching network of an inductor and a capacitor, an IC for RF communication and temperature sensing, and (optionally) a printed sensor.

An IC is needed to manage communication protocols, A/D conversion, and data storage if applicable. There are many commercially available RF and Bluetooth Systems on Chip (SoCs) that could be used. This work uses an AMS SL900A, which can be powered by a battery or run in passive mode, gathering its power from the interrogating antenna. The SL900A has a built in temperature sensor, analog input ports, an ADC, a small amount of memory, and the circuitry needed to communicate at 860-960 MHz.

### 4.1 Conductive Adhesive Materials

There are many materials that can be used for chip attachment, including solders, conductive adhesives, and inks. Solders are metal alloys that come in wire or paste form. When heated above a critical temperature, they melt (reflow) then cool to form a solid metal contact. Traditional tin-lead solder and conventional lead-free solders like tin-silver-copper are not compatible with flexible plastic substrates because the high reflow temperatures—188°C to 220°C—are above the glass transition temperature of most polymer substrates. Compositions of low temperature solder exist and can be used with most plastics. Typical low temperature solders are combinations of tin, silver, and bismuth, which have reflow temperatures between 100-150°C, such as M742 from Koki Solder Materials. Solder joints are strong, offer good electrical contact, but are rigid and brittle [16]. Components can also be attached with conductive adhesives, which, like conductive ink, are composed of conductive filler (usually silver) small particles or flakes and a polymer binder [10]. Conductive adhesives tend to have lower conductivity than printing inks because their binders, additives, and filler

percentages are chosen to improve adhesion to various substrate materials and components. Like conductive inks, conductive adhesives are usually cured with heat and pressure to fuse the separate metal particles together into a conductive network.

There are two main classes of conductive adhesives: isotropic and anisotropic. Isotropic conductive adhesives (ICAs) conduct electricity in all directions, so they must be applied (usually in a paste form) precisely at the location of each contact. Stencils or screen printing techniques can be used to apply the film. Anisotropic conductive adhesives and films have lower filler content so they conduct only in the z-direction, not in the x-y plane, therefore a single piece of film or layer of paste can be used for all the contacts of a chip without shorting different contacts together [17, 18]. Connections can also be made using nonconductive adhesives and/or non-adhesive conductors. If the conventionally packaged chip's contact pads are raised, they can pierce a thin layer of insulating adhesive to make electrical contact with the conductive trace below [19]. Another alternative is to use standard conductive ink in either inkjet or screen printable formulations [20]. Because conductive ink typically does not have the mechanical strength of a conductive adhesive, reinforcement with a nonconductive adhesive may also be necessary.

In order to determine which conductive adhesive or ink would work best with screen or stencil printed silver ink on PEN, several types of conductive adhesives, epoxies, and inks were tested. To perform these tests, RF test traces were printed with a gap of a few millimeters in one side. 0603 form factor [ $1.55 \times .85$  mm footprint] zero-ohm resistors were attached using several different materials and the RF power loss was measured using the VNA.

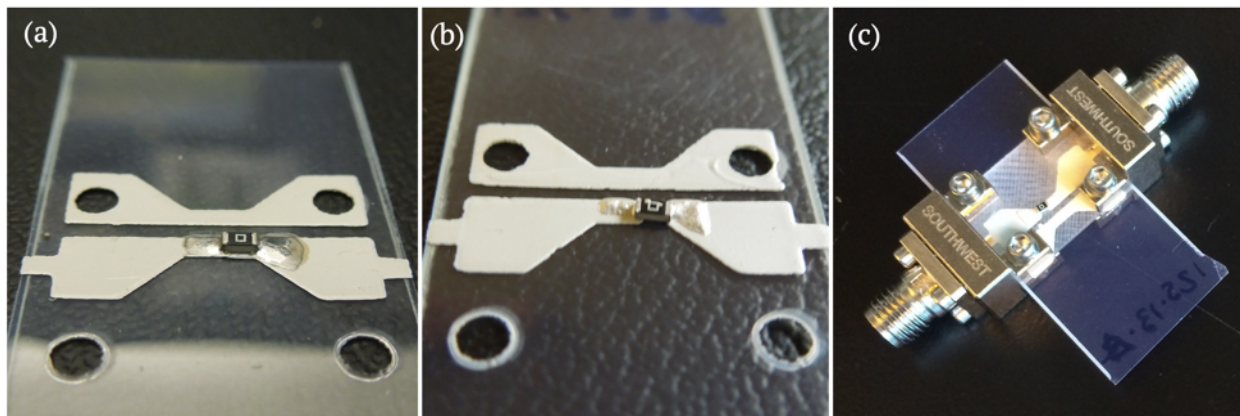


Figure 4.1: a) Zero-ohm resistor mounted with low temperature solder. b) Zero-ohm resistor mounted with screen printable silver ink. c) Test traces connected to adapters for RF cables.

The resistive losses of zero-ohm resistors connected with the various adhesives was compared to the losses of printed RF test traces with no gap to account for inherent trace and SMA connection losses. For each test material, some samples were made with the gap com-

pletely filled with the material, shorting it without a component attached. The results are shown in table 4.1.

Material	Connection Type	RF Loss at 915 MHz [dB]
none	through	-0.5
	Open	-42
Ted Pella Conductive Silver paint (PELCO # 16062)	Zero Ohm Resistor Short	-32 -5.7
MG Chemicals Silver Conductive Epoxy Adhesive	Zero Ohm Resistor Short	-1.2 -1.0
Creative Materials 125-13H Silver Screen Printable Ink	Zero Ohm Resistor Short	-0.7 -0.7
Creative Materials 120-07: Fine Features Screen Printable Ink	Zero Ohm Resistor Short	-1.2 -0.7
Koki M742 Low Melting Point Sn-Ag-Bi Solder Paste	Zero Ohm Resistor	-0.9

Table 4.1: Resistive losses at RF frequencies for several conductive adhesive materials

From these results, Creative Materials 125-13H screen printable silver ink was chosen for attaching components. Other advantages of 125-13H are its long drying time of over 30 minutes, which allows a time buffer during attachment, and ability to cleanly stencil print small features. A disadvantage of screen printing ink for attachment is that when the substrate is flexed, components can become disconnected unless an additional glue is used. In this work, Loctite 4902 flexible super glue is added to improve mechanical stability.

## 4.2 Mounting Mechanisms

Commercially available packaged ICs like the SL900A can be mounted contacts-down or contacts-up on a substrate. If the chip is mounted contacts-up, a conductor is printed over the chip and the substrate. This can be challenging because the level of the chip is above the substrate, and this step can cause disconnects. Sometimes components are embedded in a ramp material to mitigate this issue as shown in Fig 4.2a [21]. When the contacts are facing down, the solder or conductive adhesive goes between the chip and the pre-patterned substrate, as shown in Fig 4.2b. Precise alignment of chip pads to printed traces is important; a flip-chip pick-and-place tool is typically used to align chips with the conductive traces printed on the substrate. Processing parameters and materials must be chosen such that the conductive material does not spread and short the contact pads together.

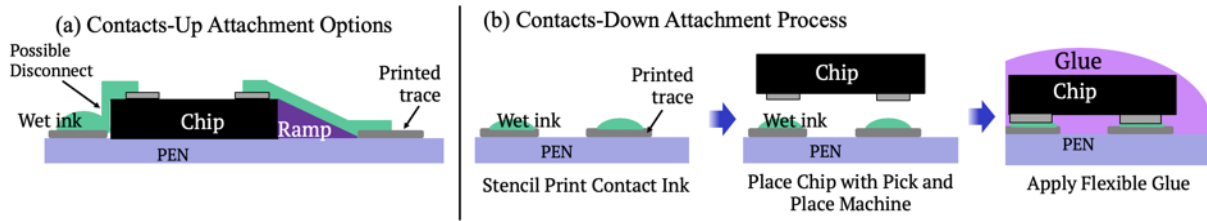


Figure 4.2: a) Contacts-up chip placement may need a ramp to prevent disconnected traces. b) Pick-and-place tools are used to align pads to traces for chips mounted contacts-down.

### 4.3 Impedance Matching

A critical step in integrating components that operate at high frequencies is impedance matching. Every element in a circuit has some complex impedance which is a function of frequency. At every place where impedance changes, a percentage of the propagating wave is reflected. These reflections limit power transfer efficiency and signal strength. In this RFID tag, the antenna and the IC need to be matched so that power received by the antenna can be used by the IC and so the signal from the IC can be transmitted by the antenna. The percent of the power that is reflected,  $P_{reflected}$  is given by equation 4.1 [13]

$$P_{Reflected} = \left( \frac{Z_L - Z_0}{Z_L + Z_0} \right)^2 \quad (4.1)$$

Where  $Z_L$  is the impedance of the load and  $Z_0$  is the reference impedance or impedance of the transmission line. A load perfectly matched to its line will have  $Z_L = Z_0$  and reflection=0. In RF circuits, it is standard to use  $Z_0 = 50 + 0j \Omega$  as a reference impedance.

The antennas were designed to have an impedance of  $50 + 0j \Omega$ . Their actual impedance can be calculated using eq. 4.1 and the S11 parameters measured by the VNA in section 3.6.  $|S11|^2$  is equal to  $P_{reflected}$  and  $Z_0$  is  $Z_0 = 50 + 0j \Omega$ , the impedance of the cables. On average, screen printed antennas have impedance of 53-6j  $\Omega$  at resonance (915 MHz).

The impedance of the IC depends on the power it receives. Mounted chip impedance was measured with the VNA by using SMA connectors to directly attach mounted chips to the VNA. The mismatch efficiency, or percent of power transferred to the chip, is shown in Fig 4.3 as a function of input power for substrate materials. The AMS demo board is a rigid printed circuit board (PCB) on FR4 which was provided by the chip manufacturer. Reference impedance data was also provided in the documentation. The flex PCB was custom ordered from a foundry which uses conventional fabrication techniques and transfers the patterns to a flexible substrate, typically polyamide. Traces are copper plated. The printed substrates were screen printed, and no impedance matching network was used.



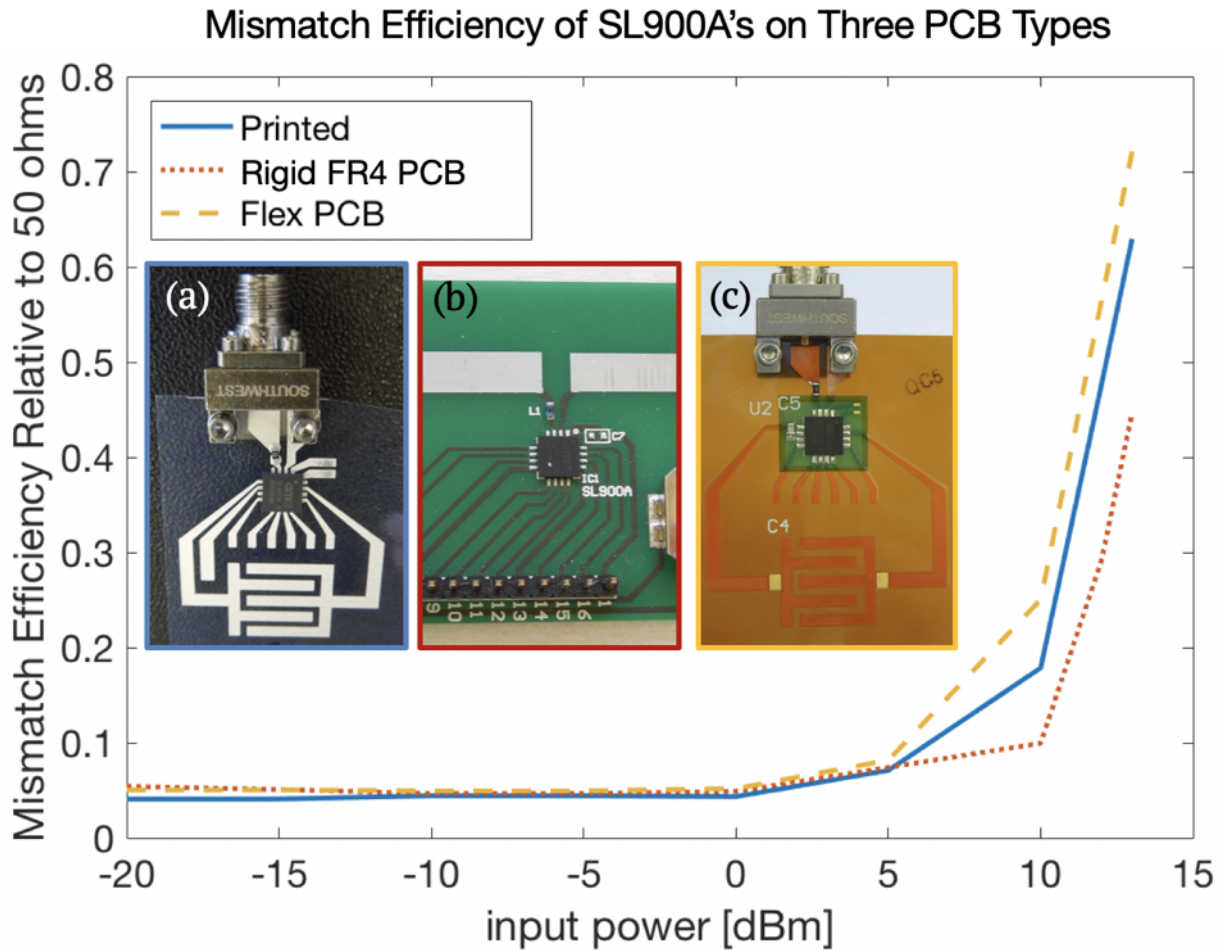


Figure 4.3: At low power, the IC impedance is about  $1.5-58j \Omega$ , causing inefficient power transfer between a  $50 \Omega$  reference and the IC. Mismatch efficiency of an IC on printed traces is similar to that of an IC on reference substrates. Insets: a) IC mounted on printed traces. b) The AMS rigid reference board. c) The flex PCB reference board;

As shown in Fig 4.3, the impedance of the IC is similar on the printed, flex PCB, and reference boards, indicating that the printed traces are not interfering with chip performance. Clearly, the mismatch efficiency is very low for input power below 5 dBm (about 3 mW), meaning that over 90% of the power is reflected. Using equation 4.1 the impedance of the chip is about  $1.5-58j \Omega$ . A matching network is needed to improve mismatch efficiency and allow the IC to transfer power to and from the antenna. A matching network is a combination of purely reactive elements chosen such that the equivalent impedance of the network and load element (the IC) equals the impedance of the antenna. Matching networks typically consist of an inductor and a capacitor. Matching networks can be made with stub transmission lines, which can be printed, but the transmission lines would need to be several cm long, and associated resistive losses might hamper performance. A matching network

made of discrete components can be custom-chosen for different applications (for example, for use on a human body or near a metal plane). Printed transmission lines do not offer this adaptability.

## 4.4 Mounting Process

First, the silver ink is stencil-printed over the printed traces as shown in Fig 4.4a. The stencil is a custom laser-cut non-adhesive polyamide (Kapton) stencil. Because this stencil is non-adhesive, it is reusable and minimum feature size is limited only by the laser beam width. Features as small as  $200 \mu m$  are possible. The stencil is larger than the substrate and both stencil and substrate are held in place by a gel-pack backing. This method works well for small features but does not work for larger features because the thin stencil is easily bent or crumpled. The thinness of the stencil reduces the total volume of ink applied, which is important to reduce spreading of fine features, as shown in Fig 4.4b.

Next, a pick-and-place die bonder is used to align the chip and impedance matching network components to the contacts on the substrate, as shown in Fig 4.4c. During bonding, the substrate is heated to  $180 \text{ }^\circ\text{C}$  to cure the silver ink. Finally, the chip is coated with a few drops of Loctite 4902 flexible super glue for mechanical stability when the tag is flexed.

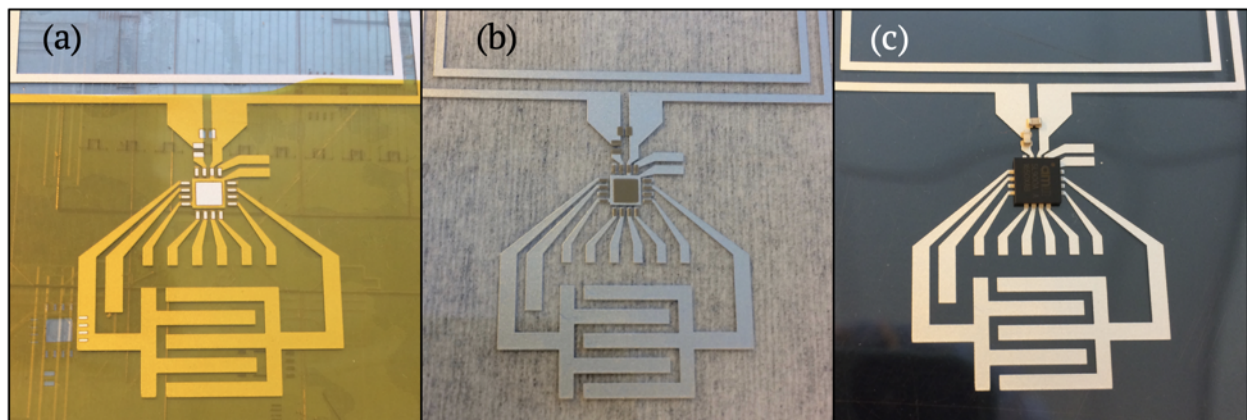


Figure 4.4: a) A laser cut stencil is used to define areas where the components will be attached to the traces. b) The wet ink after being stencil printed on the traces. c) The IC and matching network components mounted to the substrate.

# Chapter 5

## Complete RFID Tags

The functionality of the complete flexible hybrid tags was demonstrated by measuring signal strength in over the air communications and by taking temperature measurements in a controlled environment.

### 5.1 RSSI and read range

A complete passive RFID link consists of an interrogator antenna and a passive tag. The interrogator sends out an RF signal which is received by the tag. The tag harvests energy from the RF signal to power the chip, then responds by sending back data including the tag ID number and sensor data, as requested by the interrogator. The return signal strength indicator (RSSI) is a measure of the strength of the communication link. In the measurements RSSI is measured in dBm and is the power of the signal received by the interrogator from the tag.

There are many steps in this communication sequence, each with some associated loss. In the forward directions, losses include the inefficiency of interrogator antenna, free space transmission losses governed by the Friss equation (3.3), Polarization mismatch between the interrogator and tag antennas, and impedance mismatch between the antenna and chip. Each of these factors also cause loss in the return direction.

The reader antenna used in these measurements is an MT-262024/TRH/A/K from MTI Wireless Edge. It has minimum gain of 7.5 dBic, which means in the direction of maximum transmission, this antenna transmits 7.5 dB (or about 5.6 times) as much power as an isotropic source. The antenna was configured to transmit 30 dBm (1 W) of power. From section 3.6 screen printed antennas have a gain of about 0.8. The printed antennas are dipoles, which receive and transmit linearly polarized radiation, while the interrogator antenna transmits and receives right hand circularly polarized radiation. From the polarization mismatch between the interrogator and the tag, there will be a 50% loss of power in forward transmission, and another 50% reduction in the return transmission.

The RSSI of three types of tags was measured at several interrogator-tag distances.

Two rigid PCB reference boards, a commercial flex PCB tag, and five screen printed tags were measured. Each tag was placed on a Styrofoam block to minimize the influence of surrounding material, distance between interrogator and tag was incrementally increased until the signal was lost. The measurement set up is shown in Fig 5.1.

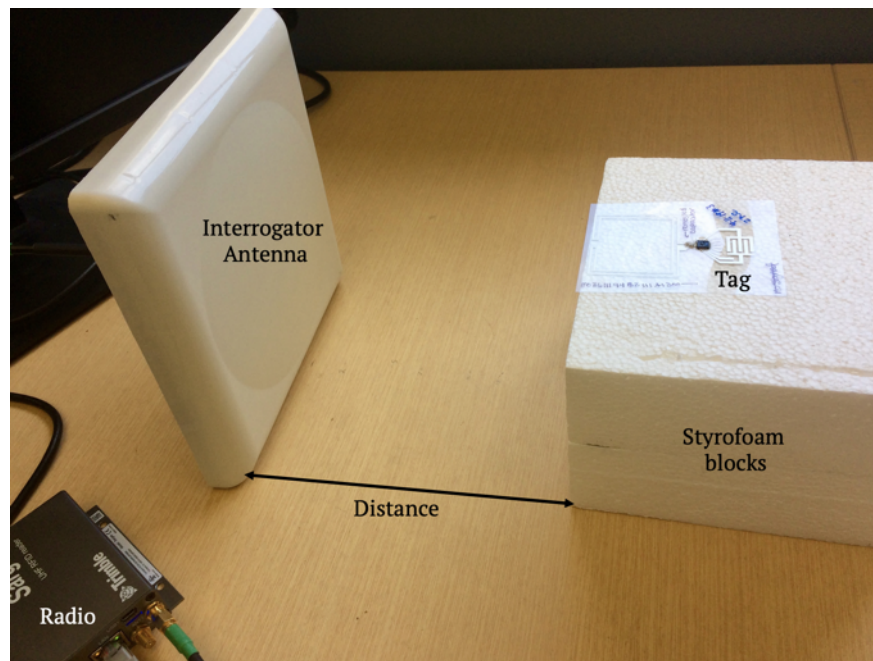


Figure 5.1: Measurement set up for RSSI and read range. The interrogator antenna sends the radio signal to the passive tag and receives the response. Successful connections were established at distances up to 40 cm.

RSSI is plotted as a function of distance in Fig 5.2. Signal strength decreases with distance, as expected from the Friis equation. Three of the printed tags, D, E, and H, behave similarly to the rigid reference boards. These samples have RSSI of -22 to -24 dBm for distances between 2 and 5 cm. At these distances,  $\lambda/d \ll 1$ , and losses from free space transmission are small. The difference between the transmitted power, 30 dBm, and RSSI, -25 dBm, is the the baseline path loss of system loss, and is determined by the factors that do not depend on distance.

Two printed samples—F and G—have significantly lower signal strength at all distances than the others. As discussed in 4.3, the impedance of the IC depends on the power it receives. Variations in surface mounted components, parasitic capacitance, and resistive losses from the mounting process impact the matching network, and thus the power received by the IC and the IC’s impedance. This is a complicated relationship.

The RSSI of the flex PCB is between -35 and -37 dBm for distances up to 35 cm. The flex PCB sample is composed of a flex PCB antenna attached with rigid SMA connectors to

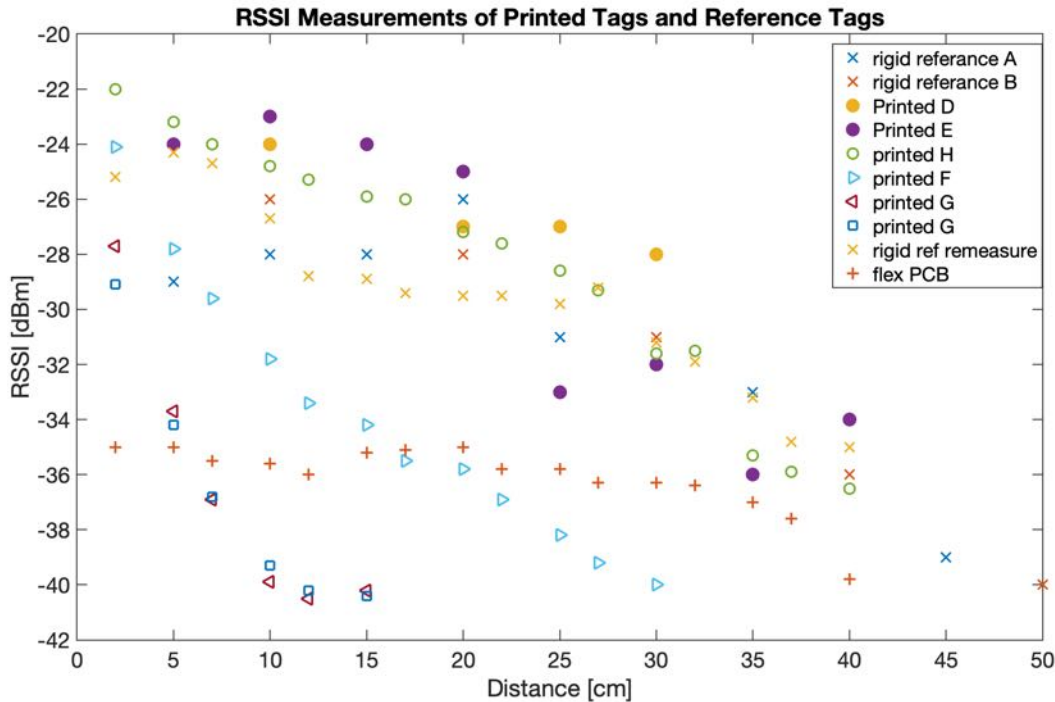


Figure 5.2: RSSI vs distance for printed and reference boards

an IC mounted on flex PCB. It is possible that losses of the connectors, which are distance-independent, dominate the free space path loss.

The SL900As used on the printed samples and flex PCB sample can be read with an RSSI as low as -40 dBm. The SL900As on the rigid PCB are a slightly different variety which can be read with RSSI as low as -60 dBm. For these comparisons, the read range is defined as the distance at which the RSSI drops below -40 dBm. The read range is about 40 cm for the printed samples and about 60 cm for the rigid PCB reference.

## 5.2 Temperature Measurements

The tags' ability to read and send sensor data was demonstrated with the SL900As' built-in temperature sensor. The interrogator antenna and two tags at a time were placed in an environmental chamber whose temperature and relative humidity can be controlled. The reader was configured to acquire temperature data and read at about 10 times per second. The temperature sensors output a voltage which is converted to a temperature through a simple linear equation given in the SL900A data sheet.

The experimental set up inside the environmental chamber is shown in Fig. 5.3. The tags are about 15 cm away from the interrogator and are approximately equally off-center



from the interrogator. The tags are set on plastic boxes and protected from being blown about inside the chamber by upright plastic boxes. The inside of the chamber is metal.

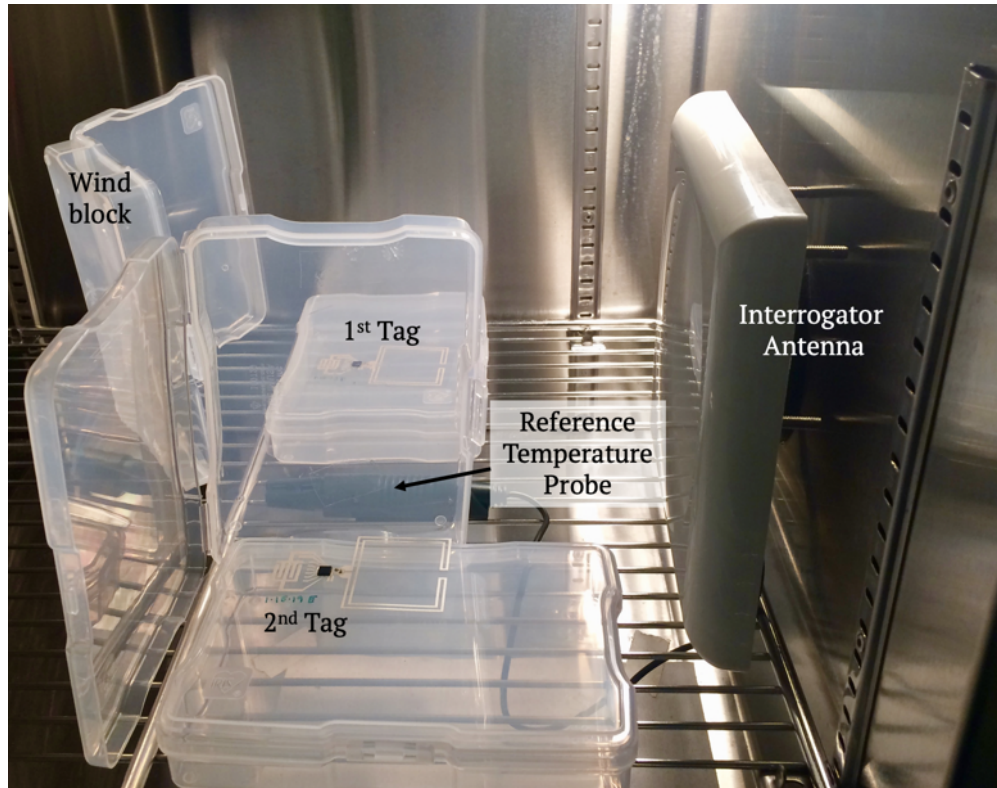


Figure 5.3: Two printed tags can send temperature data over the air to the interrogator antenna. All components of the wireless link are inside an environmental chamber.

The temperature in the chamber increased from 10°C to 30°C then decreased back to 10°C. This cycle was repeated at low (20-30 % RH), medium (45-55 % RH) and high (80-90 % RH) relative humidity. The actual temperature and humidity inside the chamber were monitored with a wired probe (RH520A from Extech Instruments). Fig 5.4a shows the temperature reported wirelessly by reference tags and Fig 5.4b shows the temperature reported wirelessly by printed tags.

The rigid reference board shows increases and decreases in temperature that align with the actual temperature changes, but tag readings have a constant offset that depends on humidity and/or running time. At low humidity, tag readers are about 8°C lower than the actual temperature, at mid humidity they are about 1°C higher, and at high humidity the tag readings are about 3°C higher than the actual temperature. At high humidity, the signal contains more frequent erroneous readings, where the signal jumps about 20°C for about one second, then returns to the correct value.

The Flex PCB signal extremely noisy and does not always follow actual temperature trends. In the low humidity temperature sweep, the tag reading drops dramatically when the

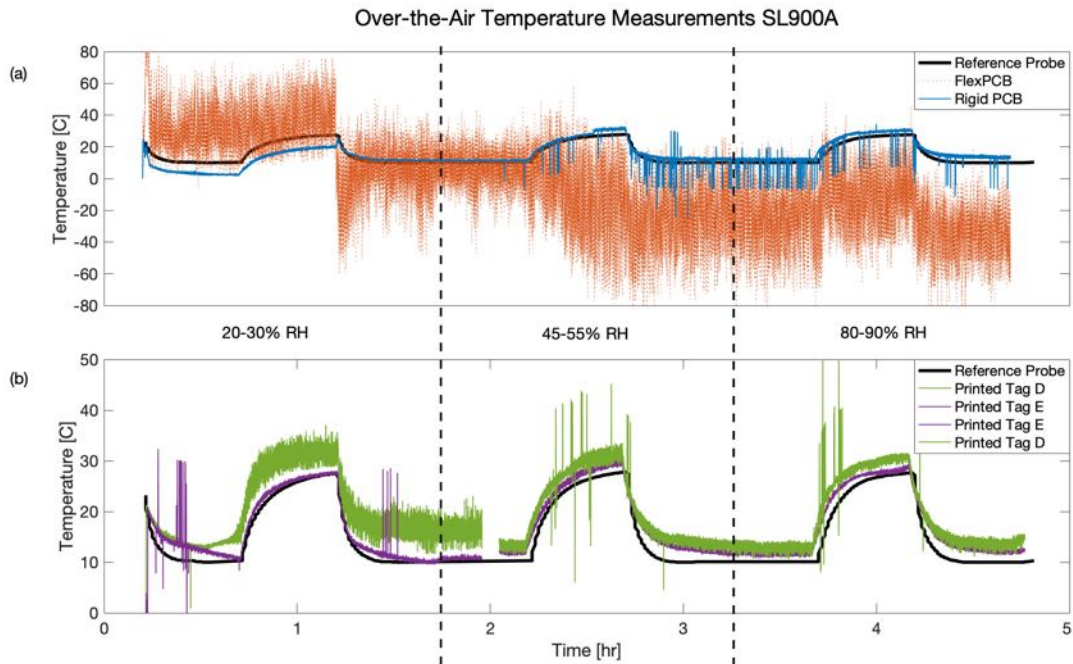


Figure 5.4: a) The rigid reference board follows relative increases and decreases in temperature well, but temperature readings are influenced by relative humidity. The signal is noisier at high humidity. The Flex PCB signal is extremely noisy and contains errors of up to  $100^{\circ}\text{C}$ . b) Both printed samples follow relative increases and decreases in temperature well and are only minorly impacted by humidity changes. Note that the printed samples were measured at two different times, which causes the small gap in the readings. Calibration would improve the absolute accuracy of the readings.

actual temperature begins to decrease. In the middle humidity range, the tag's temperature reading decreases as the actual temperature increases. When there is high humidity, the tag reading shows the correct temperature trends but they are offset by about  $50^{\circ}\text{C}$ . The high degree of noise in the signal could be caused by losses in the connection between chip and antenna. The erroneous readings are more likely due to problems with the chip, which could have been caused by high heat during mounting at the foundry.

Compared to the rigid- and flex-PCB, the printed samples have more accurate and less noisy temperature readings. Sample D has a is offset by about  $5^{\circ}\text{C}$  during warm periods and about  $2^{\circ}\text{C}$  during cool periods. The difference between sample E and the commercial reference is less than  $3^{\circ}\text{C}$ . Printed samples have less noise at higher humidity than lower humidity.

# Conclusion

Printed, flexible RFID tags have been demonstrated in the 902-928 MHz range. These tags use commercially available screen printing ink for both the antenna and the component mounting. The fabrication techniques are simple so production is scalable.

Spray coating and stencil printing can be used to prototype and characterize new antenna designs. For example, antennas operating in the 2.4 GHz range, monopole or patch antennas, or antennas whose geometries are optimized for use on the human body. These prototyping techniques allow many different designs for a new application to be easily compared. Once the antennas have been individually characterized and the most promising geometry is selected, large batch production can be done with screen printing, which also allows for the integration of discrete components.

The mounting techniques for rigid components presented here can be used for a variety of commercial or custom chips and surface mount components.

In the future, flexible printed sensors, particularly health monitoring sensors, could be integrated with the printed antenna and mounted IC to create a fully functional wireless sensor nodes.



# Bibliography

- [1] Mark Poliks et al. “A Wearable Flexible Hybrid Electronics ECG Monitor”. In: *2016 IEEE 66th Electronic Components and Technology Conference (ECTC)*. IEEE, May 2016, pp. 1623–1631. ISBN: 978-1-5090-1204-6. DOI: 10.1109/ECTC.2016.395. URL: <http://ieeexplore.ieee.org/document/7545640/>.
- [2] Claire M. Lochner et al. “All-organic optoelectronic sensor for pulse oximetry”. In: *Nature Communications* 5.1 (Dec. 2014), p. 5745. ISSN: 2041-1723. DOI: 10.1038/ncomms6745. URL: <http://www.nature.com/articles/ncomms6745>.
- [3] Yasser Khan et al. “A flexible organic reflectance oximeter array.” In: *Proceedings of the National Academy of Sciences of the United States of America* 115.47 (Nov. 2018), E11015–E11024. ISSN: 1091-6490. DOI: 10.1073/pnas.1813053115. URL: <http://www.ncbi.nlm.nih.gov/pubmed/30404911><http://www.pubmedcentral.nih.gov/articlerender.fcgi?artid=PMC6255203>.
- [4] Sarah L. Swisher et al. “Impedance sensing device enables early detection of pressure ulcers in vivo”. In: *Nature Communications* 6.1 (Dec. 2015), p. 6575. ISSN: 2041-1723. DOI: 10.1038/ncomms7575. URL: <http://www.nature.com/articles/ncomms7575>.
- [5] Yasser Khan et al. “Inkjet-Printed Flexible Gold Electrode Arrays for Bioelectronic Interfaces”. In: *Advanced Functional Materials* 26.7 (Feb. 2016), pp. 1004–1013. ISSN: 1616301X. DOI: 10.1002/adfm.201503316. URL: <http://doi.wiley.com/10.1002/adfm.201503316>.
- [6] Aminy E Ostfeld et al. “High-performance flexible energy storage and harvesting system for wearable electronics”. In: (). DOI: 10.1038/srep26122. URL: <https://www.ocf.berkeley.edu/~arias/public/publications/files/ostfeld2016high.pdf>.
- [7] Alla M. Zamarayeva et al. “Flexible and stretchable power sources for wearable electronics”. In: *Science Advances* 3.6 (June 2017), e1602051. ISSN: 2375-2548. DOI: 10.1126/sciadv.1602051. URL: <http://advances.sciencemag.org/lookup/doi/10.1126/sciadv.1602051>.
- [8] Yasser Khan et al. “Flexible Hybrid Electronics: Direct Interfacing of Soft and Hard Electronics for Wearable Health Monitoring”. In: *Advanced Functional Materials* 26.47 (Dec. 2016), pp. 8764–8775. ISSN: 1616301X. DOI: 10.1002/adfm.201603763. URL: <http://doi.wiley.com/10.1002/adfm.201603763>.

- [9] Nagarajan Palavesam et al. “Roll-to-roll processing of film substrates for hybrid integrated flexible electronics”. In: (2018). DOI: 10.1088/2058-8585/aaaa04. URL: <https://doi.org/10.1088/2058-8585/aaaa04>.
- [10] Irfan Mir and D. Kumar. “Recent advances in isotropic conductive adhesives for electronics packaging applications”. In: *International Journal of Adhesion and Adhesives* 28.7 (Oct. 2008), pp. 362–371. ISSN: 0143-7496. DOI: 10.1016/J.IJADHADH.2007.10.004. URL: <https://www.sciencedirect.com/science/article/pii/S0143749607001029>.
- [11] Vasileios Lakafosis et al. “Progress towards the first wireless sensor networks consisting of inkjet-printed, paper-based RFID-enabled sensor tags”. In: *Proceedings of the IEEE* 98.9 (2010), pp. 1601–1609. ISSN: 00189219. DOI: 10.1109/JPROC.2010.2049622.
- [12] Arno Thielens et al. “Fabrication and Characterization of Flexible Spray-Coated Antennas”. In: *IEEE Access* 6 (2018), pp. 62050–62061. ISSN: 21693536. DOI: 10.1109/ACCESS.2018.2876286.
- [13] Fawwaz Ulaby, Eric Michielssen, and Umberto Ravaioli. *Fundamentals of Applied Electromagnetics*. 6th ed. Prentice Hall, 2010.
- [14] Aniello Falco et al. “Fully printed flexible single-chip rfid tag with light detection capabilities”. In: *Sensors (Switzerland)* 17.3 (2017), pp. 1–12. ISSN: 14248220. DOI: 10.3390/s17030534.
- [15] Yi Feng et al. “Low-Cost Printed Chipless RFID Humidity Sensor Tag for Intelligent Packaging”. In: *IEEE Sensors Journal* 15.6 (June 2015), pp. 3201–3208. ISSN: 1530-437X. DOI: 10.1109/JSEN.2014.2385154. URL: <http://ieeexplore.ieee.org/document/6995967/>.
- [16] Juha Niittynen et al. “Reliability of ICA attachment of SMDs on inkjet-printed substrates”. In: *Microelectronics Reliability* 52.11 (Nov. 2012), pp. 2709–2715. ISSN: 0026-2714. DOI: 10.1016/J.MICROREL.2012.05.001. URL: <https://www.sciencedirect.com/science/article/pii/S0026271412001527>.
- [17] Henrik A. Andersson et al. “Assembling surface mounted components on ink-jet printed double sided paper circuit board”. In: *Nanotechnology* 25.9 (Mar. 2014). ISSN: 09574484. DOI: 10.1088/0957-4484/25/9/094002.
- [18] Su Tsai Lu and Wen Hwa Chen. “Reliability and flexibility of ultra-thin chip-on-flex (UTCOF) interconnects with anisotropic conductive adhesive (ACA) joints”. In: *IEEE Transactions on Advanced Packaging* 33.3 (Aug. 2010), pp. 702–712. ISSN: 15213323. DOI: 10.1109/TADVP.2010.2052806.
- [19] Guangbin Dou et al. “Thermosonic-Adhesive (TS-A) Integration of Flexible Integrated Circuits on Flexible Plastic Substrates”. In: *2018 7th Electronic System-Integration Technology Conference, ESTC 2018 - Proceedings*. Institute of Electrical and Electronics Engineers Inc., Nov. 2018. ISBN: 9781538668139. DOI: 10.1109/ESTC.2018.8546458.

- [20] J. Arrese et al. “Flexible hybrid circuit fully inkjet-printed: Surface mount devices assembled by silver nanoparticles-based inkjet ink”. In: *Journal of Applied Physics* 121.10 (Mar. 2017). ISSN: 10897550. DOI: 10.1063/1.4977961.
- [21] Yong Zhang et al. “Methods for fabrication of flexible hybrid electronics”. In: *Hybrid Memory Devices and Printed Circuits 2017*. Ed. by Emil J. List-Kratochvil. Vol. 10366. SPIE, Aug. 2017, p. 12. ISBN: 9781510611894. DOI: 10.1117/12.2275561. URL: <https://www.spiedigitallibrary.org/conference-proceedings-of-spie/10366/2275561/Methods-for-fabrication-of-flexible-hybrid-electronics/10.1117/12.2275561.full>.